minerals

Article

Quantitative Evaluation of Paleocene Reservoir Diagenetic Facies by Logging in Lishui West Sag, East China Sea Basin

Ji Teng [1,2], Qiang Fu [1,2,*], Jun Qin [3], Wenrui Ma [3], Guanyu Zhang [1,2] and Kailong Feng [1,2]

1 State Key Laboratory of Marine Geology, Tongji University, Shanghai 200092, China; tengji@tongji.edu.cn (J.T.)
2 School of Ocean and Earth Science, Tongji University, Shanghai 200092, China
3 Shanghai Branch Company of CNOOC (China) Ltd., Shanghai 200335, China; mawr2@cnooc.com.cn (W.M.)
* Correspondence: fuqiang@tongji.edu.cn

Abstract: Exploration in the Lishui West Sag of the East China Sea Basin is limited by the scarcity of offshore drilling sites, and the prediction of deep, high-quality reservoirs is challenging using only geophysical methods. This study introduces a quantitative approach to diagenetic facies division in individual wells based on logging data, providing a new method and perspective for the prediction of deep, high-quality reservoirs. We employed comprehensive data from core, logging, thin-section casting, cathodoluminescence, scanning electron microscopy, and X-ray diffraction analyses from five wells to study the petrology, physical properties, diagenetic types and strength, and diagenetic minerals of the Paleocene sandstone reservoirs in the Lishui West Sag. Apparent compaction rate, apparent cementation rate, and other quantitative characterization parameters were used to calculate the comprehensive diagenetic coefficient (C_g), and the diagenetic facies were divided into compaction, cementation, and dissolution facies. A logging calculation model for the comprehensive diagenetic coefficient (C_g) and a quantitative identification method for diagenetic facies in individual well reservoirs were established through a fitting analysis between C_g and logging curve parameters. Continuous quantitative identification of vertical diagenetic facies in the five wells in the study area showed that the high-quality reservoirs in wells L1, L2, and L3 within the L1 gas field are characterized by extensive development of dissolution facies, while wells L4 and L5 are dominated by compaction and cementation facies, with poor reservoir properties and no industrial gas flow output. The results demonstrate the reliability of the model method. The establishment of this quantitative characterization method for diagenetic facies using logging data provides guidance for the prediction of favorable reservoirs.

Keywords: diagenetic facies; diagenetic comprehensive coefficient; logging identification; East China Sea Basin; Lishui West Sag

Citation: Teng, J.; Fu, Q.; Qin, J.; Ma, W.; Zhang, G.; Feng, K. Quantitative Evaluation of Paleocene Reservoir Diagenetic Facies by Logging in Lishui West Sag, East China Sea Basin. *Minerals* **2024**, *14*, 28. https://doi.org/10.3390/min14010028

Academic Editors: Thomas Gentzis, Jingchun Tian, Qingshao Liang and Qinlian Wei

Received: 2 November 2023
Revised: 4 December 2023
Accepted: 12 December 2023
Published: 26 December 2023

1. Introduction

Diagenesis refers to a geological process in which sediments undergo a series of physical and chemical changes, such as compaction (mechanical and chemical), cementation, metasomatism, and dissolution, from the beginning of sedimentation to the end of metamorphism, under the influence of certain pressure and temperature [1–5]. Diagenetic facies comprehensively describe the type and degree of diagenesis, which is the final product of the diagenetic process. Diagenetic facies can reflect the distribution of pore type "sweet spots" in tight sandstone reservoirs and are, therefore, widely used for reservoir quality evaluation and "sweet spot" prediction [1,6,7]. However, traditional methods for studying diagenetic facies are mainly limited to core sampling, thin-section microscopy, scanning electron microscopy, cathodoluminescence, and X-ray diffraction (XRD). These research methods have many drawbacks, including high sampling costs, few samples, poor continuity, and so on [1,8–11]. In recent years, researchers have established a model for predicting diagenetic facies and reservoir quality through logging curves based on the correlation between diagenetic facies and rock physical logging curves, and conducted reservoir prediction and evaluation, achieving good results [1,5,11–16]. Logging data have the characteristics of low cost, easy acquisition, wide coverage of strata, and more complete data, which effectively compensate for the shortcomings of traditional diagenetic characteristics research. It can be used for the research and prediction of diagenesis in strata without core control.

The East China Sea Basin is the largest oil- and gas-bearing basin in China's offshore basins, and is one of the main areas for offshore oil and gas exploration in China [16–18]. Exploration has proven that the East China Sea is rich in oil and gas resources, and the exploration prospects are promising [17,19–21]. Lishui Sag is located in the southwestern part of the East China Sea Shelf Basin, with 26 drilling wells, five proven oil- and gas-bearing structures, of which nine wells have oil and gas flows and two have obtained commercial gas flow, and the Lishui West Sag, which is the focus area of the present study and the only sag that has obtained two commercial gas flow wells.

Despite the continuous oil and gas exploration activities in the Lishui Sag of the East China Sea Shelf Basin since the 20th century, research on diagenesis in this region remains sparse. The limited number of wells and scarce available data may be the primary constraints for conducting diagenesis studies in this area. In 2015, Xu Fa and colleagues, through petrological observation of the stratigraphy from different system tracts in the Mingyuefeng Formation of the Lishui Sag, discovered that the diagenetic processes in this region could be better constrained within the context of the sedimentary environment and sequence stratigraphic framework. It was proposed that an integrated approach incorporating diagenetic alteration, sedimentary environment, and sequence stratigraphy could serve as cumulative indicators to help predict reservoir quality [22]. In 2020, Liu Longlong and others conducted an in-depth study of diagenesis throughout the entire Lishui Sag. Their research results indicated that the Paleocene sandstone reservoirs in the Lishui Sag have poor physical properties, with an average porosity of 11.3%, but are dominated by ultra-low-porosity permeability. Sedimentary microfacies are the primary controlling factors in forming high-quality reservoirs. Compaction and carbonate cementation are the main reasons for the decrease in porosity and permeability, whereas the impact of clay mineral cementation on reservoir quality may not be significant. In contrast, dissolution processes contribute to the formation of favorable reservoirs [23].

2. Geological Setting

The total area of the East China Sea shelf basin is 267,000 km^2, with a maximum sedimentary thickness of 9000–15,000 m, mainly composed of Cenozoic strata [18–21]. The East China Sea shelf basin is a typical backarc rift basin, further divided by a series of depressions and basement ridges. Its structural units can be divided into the eastern depression belt, central uplift belt, and western depression belt. The eastern sag belt includes Diaobei Sag, Xihu Sag, and Fujiang Sag. The central uplift belt is composed of Hupijiao Uplift, Haijiao Uplift, and Yushan Uplift. The western sag belt is composed of Pengjiayu Sag, Lishui Sag, Fuzhou Sag, Jiaojiang Sag, Qiantang Sag, etc. [18,19,24–28] (Figure 1A).

Lishui Sag is located in the southwest edge of the East China Sea shelf basin, the west and south of which is the NNE-trending Minzhe Uplift structural belt, the east is the Yandang Ridge, and the north is adjacent to the Jiaojiang Sag, with a total area of 13,785 km^2, and a general trend of the NNE [20,29–31]. The geological structure of the Lishui West Sag is characterized by an eastern fault and a western overlap, with a relatively gentle slope at the western edge of the basin. It is mainly composed of tilted fault blocks, which were formed by the development of reverse normal faults. During the mid-Paleocene, these geological faults reached their peak tectonic activity. As the period transitioned into the late-Paleocene epoch, there was a progressive reduction in crustal activity, marked by a noticeable slowdown in extensional activities. By the end of the Paleocene, fault activities had largely ceased, and their influence over deposition became less significant. Overall, the

Lishui Sag is divided into two subsags, east and west, separated by the Lingfeng Ridge of the central buried hill drape structural belt. Further division allows the Lishui Sag to be classified into five sub-structural units: Lishui West Sag, Lishui East Sag, Lishui South Sag, Lingfeng Ridge, and Lishui South Ridge [18–20,27,29,32] (Figure 1B).

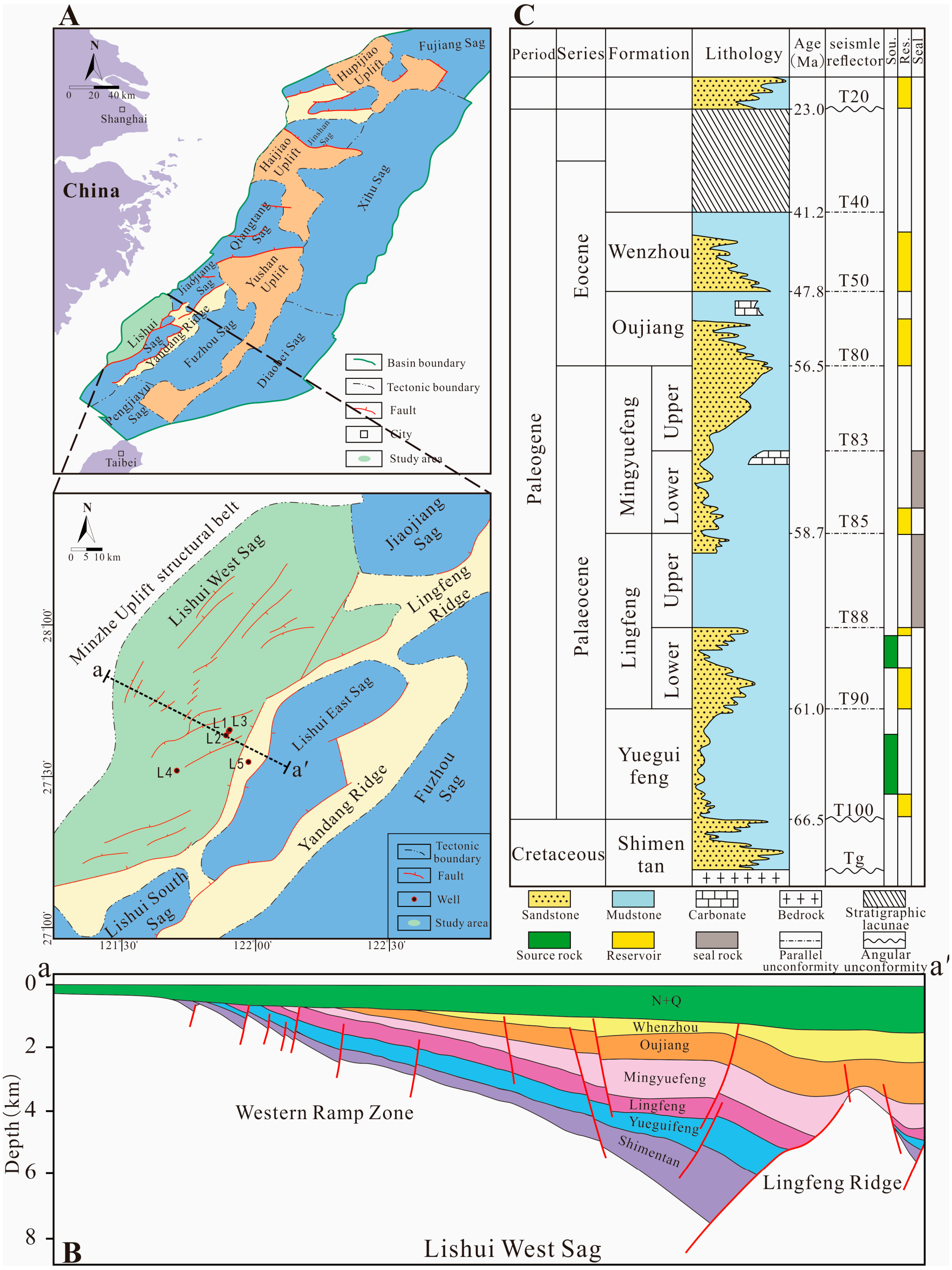

Figure 1. Location (**A**), tectonic setting (**B**) and stratigraphic units (**C**) of the Upper Cretaceous to Eocene in the Lishui Sag (according to [30] (revised)).

The Lishui West Sag is the main sag of the Lishui Sag, with an area of approximately 15,000 km^2 and a maximum sedimentary thickness of up to 12,000 m. The subsidence center of the Lishui Sag is mainly located on the descending plate of the Lingfeng Fault in the eastern part of the Lishui West Sag, and the sedimentary thickness of the Lishui Sag is controlled by the segmented activity of the Lingfeng Fault, with uneven filling characteristics (Figure 1C).

The Paleocene strata in the Lishui West Sag can be divided into the Yueguifeng Formation, Lingfeng Formation, and Mingyuefeng Formation from old to new. In terms of the reservoir–cap rock system, the marine mudstone of the Paleocene Yueguifeng Formation is the main source rock, the marine mudstone of the Lingfeng Formation is the secondary source rock, the sandstone body of the Mingyuefeng Formation is the reservoir, and the thick mudstone in the middle and upper parts of the Mingyuefeng Formation is the regional cap rock. The target interval of this study is the Paleogene system, including the Paleocene Mingyuefeng Formation and Lingfeng Formation, which are the reservoir and sealing strata of oil and gas reservoirs [21,25–28,31,32].

During the Paleocene sedimentary period in the Lishui West Sag, three major depositional facies were formed: fan-delta, delta, and shallow marine (or shallow lacustrine). The subfacies of the delta plain and delta front are widely distributed along the slope zone in the west. Influenced by the Lingfeng ridge, the fan-delta facies is extensively developed in the eastern part. The shallow marine (or shallow lacustrine) environment, on the other hand, predominantly characterizes the LS36 subsag [33].

3. Materials and Methods

3.1. Well Logging Data and Experimental Procedures

The conventional logging series in Lishui West Sag includes gamma ray logging (GR), caliper logging (CAL), neutron porosity (CNL), volume density (DEN), acoustic time difference (AC), and spontaneous potential (SP). This study mainly selected volume density (DEN) and gamma ray logging (GR), and correlated DEN characteristics with cored testing results to perform core logging depth matching, followed by quantitative characterization of diagenetic facies through logging. More than 40 samples extracted from 5 core wells were used for routine core analysis, the core plug helium porosity and air permeability were measured at confining pressures of 800 psi (5.5 MPa) net effective stress. A total of 35 samples were selected and thin sections were made using blue resin impregnation and staining with alizarin red S and K potassium ferrocyanide. Observations were conducted using plane-polarized light and cross-polarized light to identify the composition, structure, and structural maturity of rocks, the composition, grain size, and packing density of grains, and the type and volume of pores, and to identify carbonate minerals (calcite, ferrodolomite, and ferrocalcite). Rock and clay components (<2β m) and the XRD method were used to analyze the clay mineral content (weight percentage) to determine the semi-quantitative mineral composition (quartz, feldspar, carbonate). A total of 50 representative samples were examined using scanning electron microscopy (SEM) and the images were analyzed (at 15 to 20 kV acceleration voltages with beam currents of 1 and 0.6 nA). These data were used to determine the pore structure and the presence of different clay minerals, authigenic quartz, carbonate cements, etc., within the pores, and their diagenetic processes were analyzed. In addition, a cold cathodoluminescence mirror was used to perform cathodoluminescence (CL) analysis on 10 polished thin films to determine cementation, grains and timing of cementation (voltage 14.2 kV).

3.2. Quantitative Evaluation Methods of Diagenetic Facies

Quantitative characterization of diagenetic facies is typically achieved through quantitative diagenesis, a perennially hot and cutting-edge topic in reservoir-related research [34]. To quantitatively illustrate the impact of mechanical compaction and cementation on the original pore volume, the following formula is used:

$$R_p = \frac{40 - V_p}{40}$$

$$R_c = \frac{V_c}{V_c + V_\varphi}$$

In the formula, "R_p" is the apparent compaction rate, "R_c" is the apparent cementation rate, "V_p" is the volume between grains after compaction, "V_c" is the volume of the cement, and "V_φ" is the volume of intergranular pores. During diagenetic evolution, reservoirs undergo multiple diagenetic processes like compaction, cementation, and dissolution. Different diagenetic processes alternate or occur simultaneously, forming current diagenetic facies characteristics. Thus, some scholars have summarized the diagenetic comprehensive coefficient methods to quantitatively characterize diagenesis, including compaction, cementation, and dissolution [35–41]:

$$R_m = \frac{\varphi_f - m}{\varphi_f}$$

$$C = \frac{m}{R_p + R_c + R_m}$$

In the formula, "R_m" is the micro-pore rate, "φ_f" is the physical porosity, "m" is the surface pore rate, and "C" is the diagenetic comprehensive coefficient. Yangning improved this method by introducing the parameter of packing density of grains in 2014 [36]:

$$C_g = \frac{D_f}{R_p + R_c + R_m} \times m$$

This improved calculation method for the diagenetic comprehensive coefficient can better reveal changes in diagenetic facies under the influence of multiple diagenetic processes.

4. Results

4.1. Petrology Characteristics

Thin-section analysis of five wells in the Paleocene series of Lishui West Sag revealed that the reservoir is primarily litharenite (>95% of the total), followed by feldspathic litharenite (Figure 2A,B). Quartz volumes vary from 5% to 57% (average 27%), predominantly single crystal. Feldspar fractions range from 5% to 49% (average 19.8%), with plagioclase as the majority and potassium feldspar in lesser amounts. Rock fragment volumes span from 5% to 85% (average 53.6%), mostly igneous and metamorphic, with fewer sedimentary fragments. The fillings' volumes range from 3% to 21.3%, with average fractions of 5.3% for the matrix and 9.5% for the cements. Grains are chiefly fine-to-medium sand, moderately sorted, poorly rounded, with line contact and concave–convex contact as the primary grain interconnections (Figures 2C and 3).

4.2. Reservoir Physical Property

According to measurements of the core samples, the reservoir quality of the Mingyuefeng and Lingfeng Formations is poor, with low porosity and permeability. The reservoir's pore structure is mainly characterized by small pores and fine throats, with a mixed composition of primary and secondary pores, including intergranular, intragranular, mold pores, cracks, and micro-pores (Figure 2D). Porosity ranges between 0.01% and 26.00%, averaging at 11.3%, with 64.9% of samples exceeding 10%. Permeability spans from 0.01×10^{-3} μm^2 to 248×10^{-3} μm^2, averaging 10.32×10^{-3} μm^2, with 32.6% of samples falling below 1×10^{-3} μm^2 (Figure 4). In the Paleocene reservoirs of the Lishui West Sag, primary porosity accounts for 34% to 70% of the total porosity, while secondary porosity makes up 28% to 43% of the total porosity. Micro-porosity and micro-fractures contribute 0% to 23% to the total porosity (Figure 5).

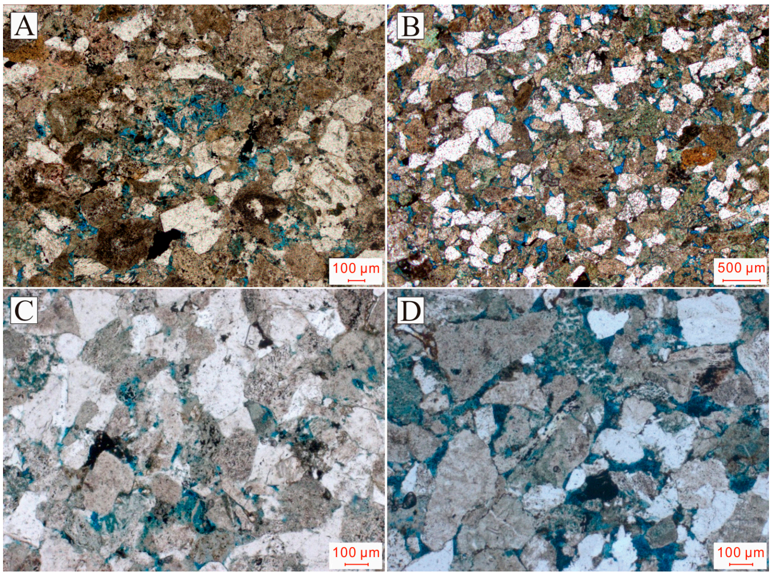

Figure 2. Photomicrographs showing the petrology characteristics of the Paleocene reservoir in Lishui West Sag. (**A**) L3 well, 2744 m, fine-grained lithic sandstone; visible dissolution of feldspar to form pores. (**B**) L1 well, 2580.55 m, fine grained feldspar lithic sandstone; the grains are aligned parallel to long axis as a result of compaction. (**C**) L3 well, 2746.16 m; strong compaction effect, with concave–convex contact between grains. (**D**) L1 well, 2258.64 m; strong dissolution forms intraparticle and intergranular dissolved pores.

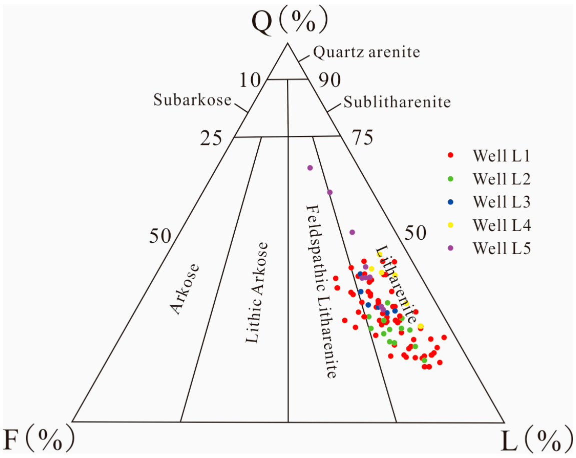

Figure 3. Composition triangle of Paleocene sandstone in West Lishui Sag.

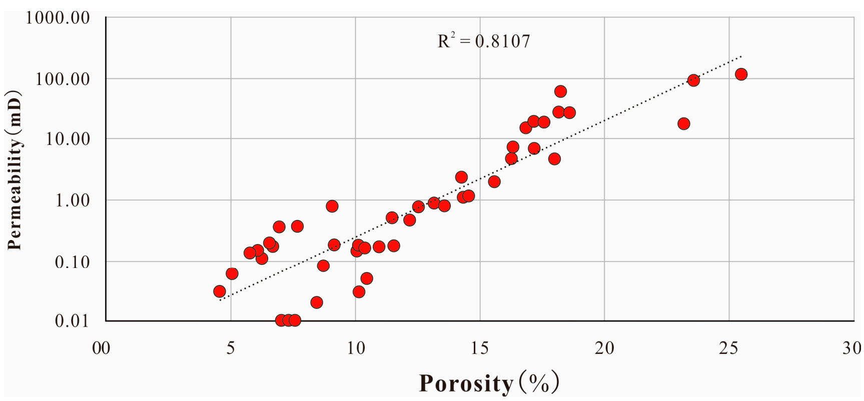

Figure 4. Core porosity versus core permeability cross-plots for Paleocene reservoirs in Lishui West Sag.

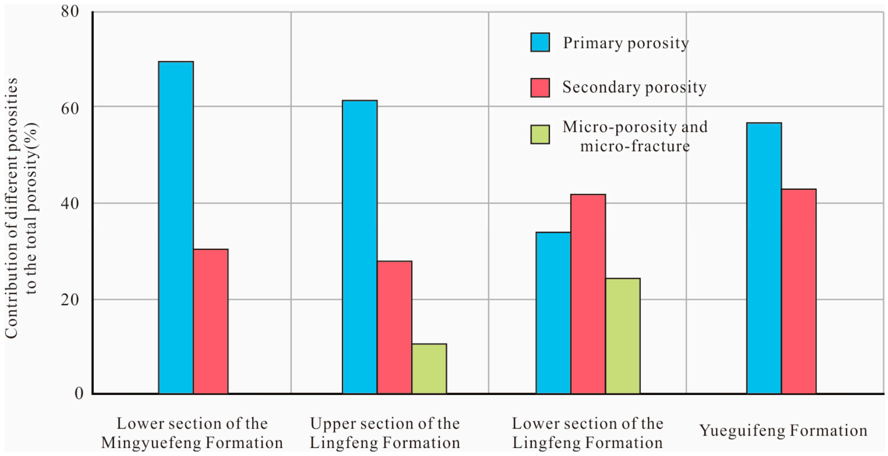

Figure 5. Pore volume distribution chart of Lishui West Sag.

4.3. Diagenesis Type of Reservoir

Through ordinary thin sections, cast thin sections, scanning electron microscopy, and cathodoluminescence analysis, it was found that the Paleocene sandstone reservoir in Lishui West Sag mainly underwent destructive diagenesis such as compaction and cementation, as well as positive diagenesis caused by dissolution. Currently, it is in the mesodiagensis A stage (Figure 6).

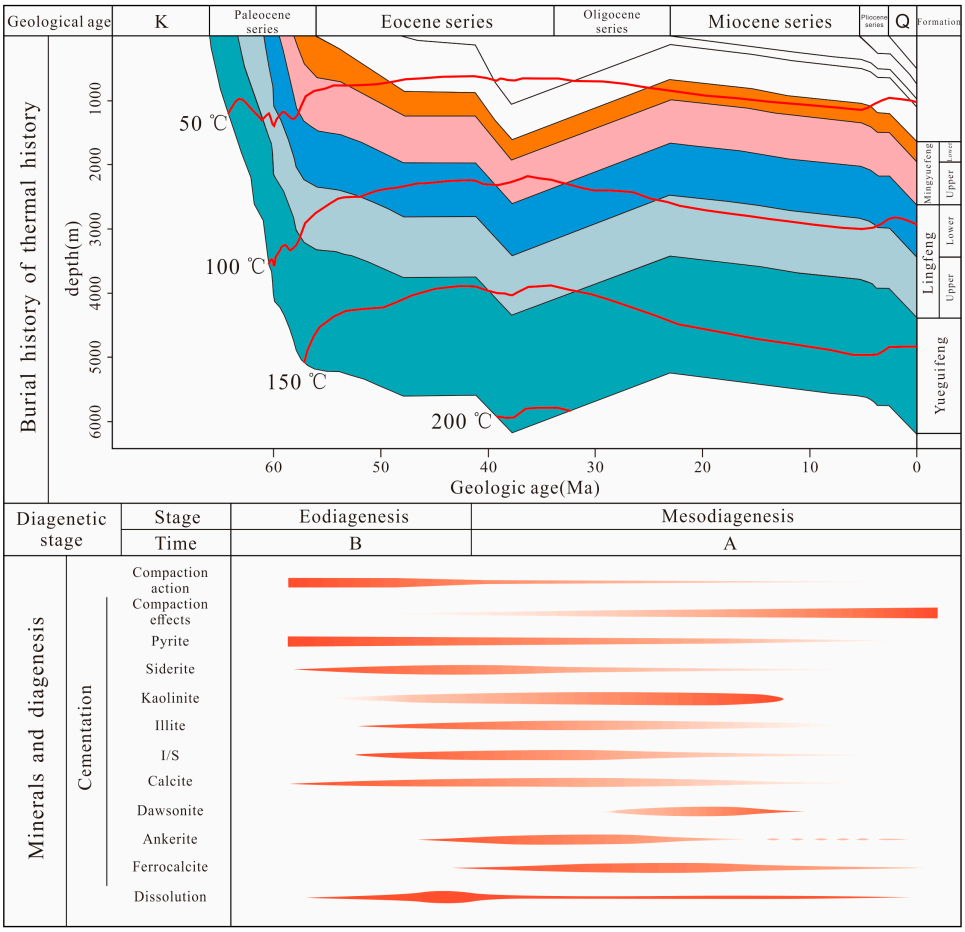

Figure 6. Thermal burial history of diagenetic sequence in Lishui West Sag (the thermal history burial history data were sourced from internal data of Shanghai Branch Company of CNOOC).

4.3.1. Compaction

The compaction of the Paleocene reservoir sandstone in Lishui West Sag is predominantly attributed to mechanical compaction [21,25]. With a low volume fraction of quartz and feldspar grains and a high content of volcanic fragments, the reservoir exhibits weak mechanical compaction resistance and pronounced compaction effects. Stratigraphically, the deeper Yueguifeng Formation and Lingfeng Formation are more significantly affected by compaction than the Mingyuefeng Formation. Existing thin-section data analysis and microscopic observation of cast thin-sections reveal the compaction effect mainly as follows: ① Clastic grains experience directional compaction, with their long axis reordered towards a direction close to horizontal (Figure 7A), a phenomenon common in the Mingyuefeng Formation. ② Plastic grains deform, with mica, glauconite, and bioclast bending and elongating post-compaction. Under strong compaction, they can be crushed or even become a pseudomatrix (Figure 7B). This phenomenon is observable in the upper sections of the Mingyuefeng Formation and Lingfeng Formation. ③ Rigid grains such as quartz and feldspar fragment along the cleavage surface post-compaction. This phenomenon is found in the lower part of the Lingfeng Formation and the Yueguifeng Formation, albeit at a relatively low frequency. ④ The contact relationship between grains alters with the intensity of compaction, and as the depth increases, the compaction gradually strengthens. Grains approach each other from a separated state and tend to become more compact. Initially, the clastic grains mainly have point-line contact (mostly found in the Mingyuefeng Formation), progressing to surface contact (mostly found in the Lingfeng Formation and Yueguifeng Formation) and concave–convex contact (mostly found in the Yueguifeng Formation) (Figure 7C). Quartz and feldspar fragments undergo pressure dissolution due to compression, significantly reducing reservoir porosity and permeability.

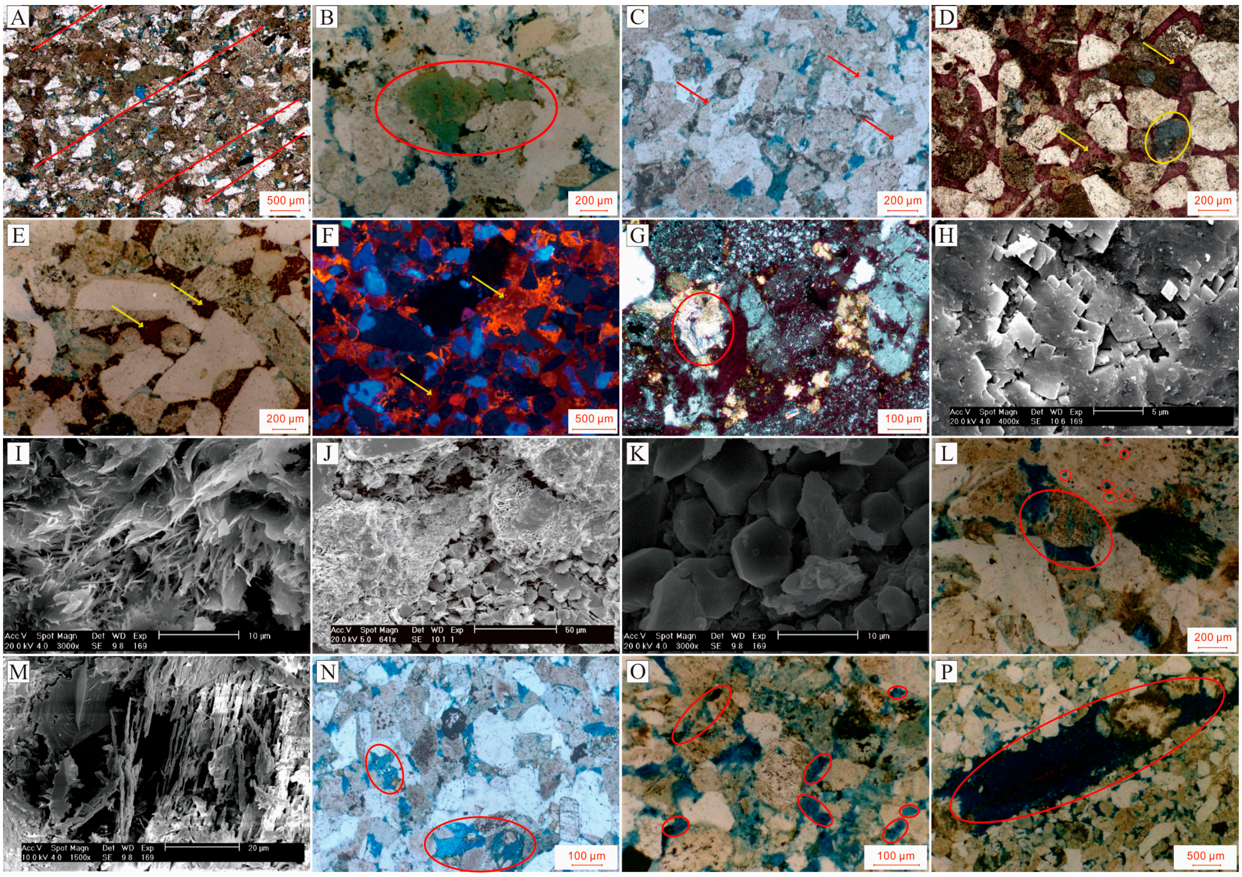

Figure 7. Photomicrographs showing the microscopic diagenetic features of Paleocene reservoirs. (**A**) L3 well, 2744 m. The grains are aligned parallel to long axis as a result of compaction. (**B**) L1 well,

2581.03 m. Glauconite undergoes deformation after being compacted. (**C**) L4 well, 3761.9 m. After strong compaction, the grains come into concave–convex contact. (**D**) L4 well, 3345.3 m. The intergranular pores are completely filled with ferrocalcite and ferrodolomite. (**E**) L1 well, 2444 m. The intergranular pores are completely filled with ferrocalcite. (**F**) L2 well, 2245.2 m. Ferrocalcite filling pores emitting orange-red light. (**G**) L2 well, 2293.63 m. Dawsonite is radially filled with pores. (**H**) L4 well, 3365.98 m. Authigenic illite filling pores, with visible micro-pores inside. (**I**) L4 well, 3322.8 m. Authigenic illite filling pores, with visible micro-pores inside. (**J**) L3 well, 2740.76 m. The intergranular pores are filled with kaolinite and illite. (**K**) L2 well, 2247.2 m. Authentic quartz filling pores with visible micro-pores. (**L**) L1 well, 2370.5 m. Internal dissolution of grains produces intragranular pores. (**M**) L2 well, 2291.54 m. Formation of pores by dissolution of feldspar. (**N**) L3 well, 3354.72 m. Complete dissolution of quartz and feldspar to form mold pores. (**O**) L1 well, 2270 m. Dissolution produces intergranular pores. (**P**) L1 well, 2579.07 m. The pores formed by dissolution of plant fragments are filled with dawsonite.

4.3.2. Cementation

The cementation in the Paleocene reservoir of Lishui West Sag encompasses carbonate, clay mineral, and siliceous types [21,25]. Detailed analysis, including thin-section observation, scanning electron microscopy, and cathodoluminescence observation, reveals the following: ① Carbonate cements are prevalent in the Paleocene reservoirs of Lishui West Sag, significantly influencing reservoir property alterations. Composed mainly of ferrocalcite and ferrodolomite, minor siderite, and a trace of dawsonite (Figure 7D–G,H), ferrocalcite, although not abundant, completely fills the pores in samples with high content. It indicates a late precipitation phase and does not contribute to enhancing the compaction resistance. Its concavo-convex contact with clastic grains impairs the reservoir's physical properties. Ferrodolomite, related to burial depth and reservoir temperature, is predominantly found in the Mingyuefeng Formation. Despite high ferrodolomite content in some samples, high porosity remains, implying early-stage precipitation before effective rock compaction, hence positively affecting compaction resistance. Dawsonite, primarily developed in the Mingyuefeng Formation, occupies solution pores of feldspar and rock fragments, indicating a late formation. ② Clay minerals are predominantly kaolinite and illite, followed by mixed-layer I/S and negligible chlorite and montmorillonite (Figure 7I,J). Clay minerals significantly impair the reservoir's porosity and permeability. Kaolinite, developed in the upper part of Mingyuefeng and Lingfeng Formations, fills intergranular pores, while illite, present in various strata, fills pores or covers grain surfaces. The mixed-layer I/S, with a morphology between illite and montmorillonite, is present across the Paleocene strata in Lishui West Sag. ③ Siliceous cementation is less developed and comprises mainly quartz overgrowths and authigenic quartz (Figure 7K), with surrounding clay minerals limiting quartz growth.

4.3.3. Dissolution

The Paleocene reservoir in Lishui West Sag, following intense compaction, generated numerous secondary pores via dissolution, alongside residual primary ones, improving the reservoir's physical properties [21]. Thin-section microscope observations reveal: ① Feldspar dissolution, widespread across Lishui West Sag's Paleocene strata, leads to intergranular and intragranular dissolved pores with distinct honeycomb-like, harbor-like, or serrated edges (Figure 7L,M). Some sections show quartz particle dissolution, forming mold pores (Figure 7N). ② Rock fragment dissolution, common in the Paleocene reservoir, results in partial volcanic fragment dissolution and bioclastic dissolution leading to intergranular dissolved pores (Figure 7O). Some sections show complete bioclastic dissolution, forming mold pores (Figure 7P). ③ Diagenetic mineral dissolution is less frequent and extensive, with its resultant pores minimally improving the reservoir's properties and secondary pore formation.

5. Discussion

5.1. Characteristics and Classification of Reservoir Diagenetic Facies

At present, there is no unified classification and naming method for diagenetic facies. Different scholars mainly classify diagenetic facies based on diagenesis, diagenetic minerals, and diagenetic evolution sequences [1,12,25,42–44]. On the basis of previous quantitative characterization of diagenetic facies parameters, this study referred to the diagenetic comprehensive coefficient method and classified the diagenetic facies using the three diagenetic processes that have the greatest impact on reservoir physical properties, namely compaction, cementation, and dissolution. The characteristics of different diagenetic facies were comprehensively described based on quantitative characterization parameters such as apparent compaction rate, apparent cementation rate, and micro-pore rate. We established a quantitative classification standard for the diagenetic facies of the Paleocene reservoir in Lishui West Sag (Table 1).

Table 1. Diagenetic facies quantitative criteria for classification.

Diagenetic Facies	Surface Pore Rate M (%)	Apparent Compaction Rate R_p (%)	Apparent Cementation Rate R_c (%)	Micro-Pore Rate R_m (%)	Filling Density D_f (%)	Diagenetic Comprehensive Coefficient (%)
Compaction facies	0.1~12.4	63.9~97.8	10.3~99.7	63.5~98.3	93.6~98.7	<1.82
Cementation facies	1.3~9.8	36.2~73.4	67.1~99.8	28.4~94.3	89.2~99.6	1.82~3.7
Dissolution facies	3.1~14.5	17.3~72.5	8.3~65.4	17.9~48.1	79.3~91.5	>3.7

Compaction facies (Figure 8): The main contact between grains is concave–convex, with the development of intergranular pores. Some intergranular pores are filled with cements, resulting in a higher apparent cementation rate of the cast thin section. The apparent compaction rate ranges from 63.9% to 97.8%, the apparent cementation rate ranges from 10.3% to 99.7%, the micro-pore rate ranges from 63% to 98.3%, and the range of the C_g is less than 1.82%.

Cementation facies (Figure 8): Mainly carbonate cementation, followed by clay mineral cementation and less siliceous cementation. The carbonate cement is composed of ferrocalcite and ferrodolomite, while the clay mineral cements are mainly composed of kaolinite and illite. The casting thin section reveals that the extensive development of carbonate cementation significantly reduces primary and secondary pores. The apparent compaction rate ranges from 36.2% to 73.4%, the apparent cementation rate ranges from 67.1% to 99.8%, the micro-pore rate ranges from 28.4% to 94.3%, and the range of C_g is from 1.82% to 3.7%.

Dissolution facies (Figure 8): Dissolution is extensively developed in the reservoir, greatly improving the physical properties of the reservoir. Intergranular dissolution pores, intragranular dissolution pores, and mold pores, typically resulting from the dissolution of feldspar or rock fragments, are frequently identified on cast thin sections. The apparent compaction rate ranges from 17.3% to 72.5%, the apparent cementation rate ranges from 8.3% to 65.4%, the porosity rate ranges from 17.9% to 48.1%, and the range of the C_g is greater than 3.7%.

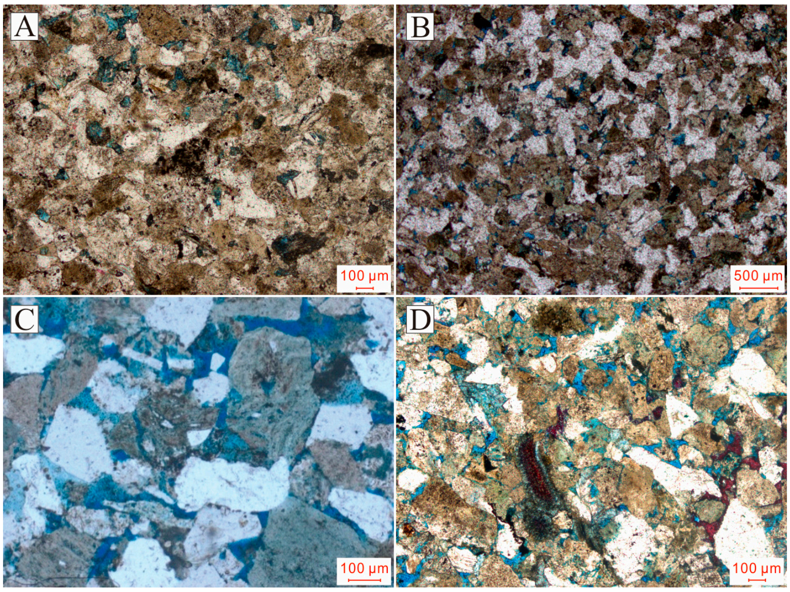

Figure 8. Cast thin-section characteristics of diagenetic facies in Paleocene Formation. (**A**) L4 well, 3341.4 m. Apparent compaction rate = 87.3%, apparent cementation rate = 97.1%, micro-pore rate = 97.7%, C_g = 0.07%, and compaction facies; (**B**) L4 well, 3334.8 m. Apparent compaction rate = 88.3%, apparent cementation rate = 31.1%, micro-pore rate = 43.2%, C_g = 1.52%, and compaction facies; (**C**) L2 well, 2253.41 m. Apparent compaction rate = 49.5%, apparent cementation rate = 57.1%, micro-pore rate = 33.3%, C_g = 5.59.6%, and dissolution facies; (**D**) L1 well, 2580.55 m. Apparent compaction rate = 43.2%, apparent cementation rate = 99%, micro-pore rate = 96.3%, C_g = 1.79%, and cementation facies.

5.2. Quantitative Characterization Method for Diagenetic Facies Logging

The key problem in identifying diagenetic facies lies in the interval without core sampling, and logging data have the characteristics of low cost, easy acquisition, strong continuity, and wide coverage, giving the logging response identification of diagenetic facies broad application prospects. The differences in structure, composition, and physical properties of different types of diagenetic facies result in their different response characteristics on logging curves, which is the theoretical basis for identifying and detecting diagenetic facies using logging curves [5,35]. However, it is worth noting that the porosity and permeability of sandstone gradually decrease as the burial temperature increases from the surface to 150 degrees Celsius, with little change at higher temperatures. According to the burial depth, the diagenetic temperature of the high-quality reservoir studied this time is between 96 and 106 degrees Celsius, with little overall temperature variation [45]. Therefore, based on the correlation between logging response and diagenetic facies, a logging diagenetic facies discrimination model and evaluation method can be established, and favorable reservoirs can be identified to achieve the qualitative and quantitative prediction of diagenetic facies by logging [1,16,23,25].

After matching the thin-section identification data with the logging depth, we read the corresponding logging curve values, established a correlation analysis between DEN and porosity, and obtained a physical property analysis (porosity φ) calculation model. Then, we analyzed the correlation between C_g and the physical property analysis (porosity φ)/mudstone content in the logging curves (V_{sh}) and found a significant correlation between the two (Figure 9). The data points exhibit a bi-modal distribution, which may be attributed to the combined effects of compaction and cementation deteriorating the physical properties, contrasted with the beneficial enhancement of reservoir properties due to dissolution processes. This results in the data points clustering around two distinct values, thereby presenting a pronounced bi-modal characteristic. Therefore, C_g can be calculated through logging curves and continuously quantitatively dividing diagenetic facies for a single well.

$$\varphi = -55.923DEN + 148.19 \tag{1}$$

$$V_{sh} = \frac{GR - GR_{min}}{GR_{max} - GR_{min}} \times 100\% \tag{2}$$

In the equation, "φ" Is the porosity, "DEN" is the logging density value at a specific depth, "V_{sh}" is the mudstone content (%), "GR" is the natural gamma value of the logging at a specific depth, "GR_{min}" is the minimum density value of the target layer pure sandstone well section logging, and "GR_{max}" is the maximum density value of the target layer pure mudstone well section logging. If the mudstone content is >40%, the porosity is automatically assigned a value of 0.1%.

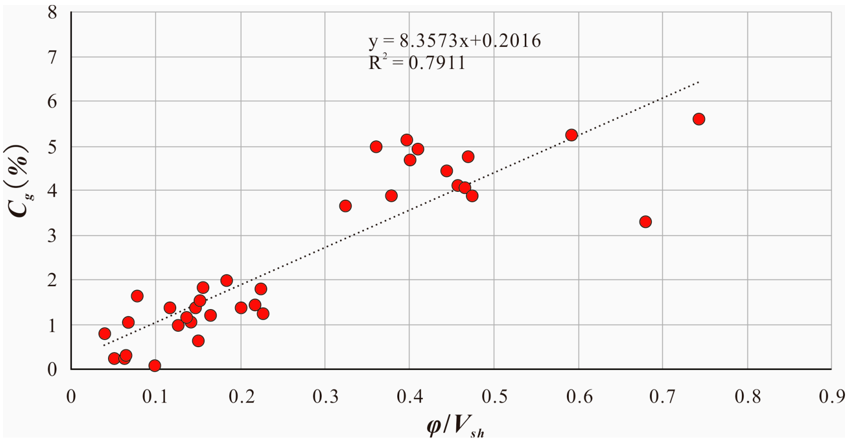

Figure 9. Fitting diagenetic comprehensive coefficient and well logging curve.

5.3. Single-Well Diagenetic Facies Discrimination

Based on the analysis of diagenetic facies types and the quantitative characterization method of diagenetic facies logging, a logging data identification model was established to study the vertical distribution pattern of single-well diagenetic facies in Lishui West Sag. Taking the Paleocene reservoir of five wells in Lishui West Sag, including L1, L2, L3, L4, and L5, as an example, the porosity, mudstone content, and diagenetic comprehensive coefficient (C_g) were calculated through logging interpretation to classify the diagenetic facies of a single well. Finally, casting thin sections were used to verify the effectiveness of the identification, and it was found that the identification effect was good, which has good application potential for the Paleocene reservoir in Lishui West Sag (Figure 10).

The L1 and L2 wells are located inside the LS36 subsag in the southern part of Lishui West Sag, with the Paleocene reservoir depths ranging from 2000 to 4500 m. The diagenetic facies of the reservoir are mainly compaction facies, which can reach a maximum thickness of 11.6 m. The dissolution facies are also relatively developed, which can reach a maximum thickness of 7.8 m. The development of cementation facies is relatively concentrated, mostly alternating with the dissolution facies in the vertical direction to develop. The casting thin section also shows typical characteristics of compaction facies and dissolution facies. The grains in the compacted faces casting thin section show concave–convex contact, with little or almost no development of cementation and dissolution. The cementation facies casting thin section can be seen filling pores with ferrocalcite and ferrodolomite, while the dissolution facies casting thin section is mainly composed of intergranular and intragranular dissolved pores (Figure 10).

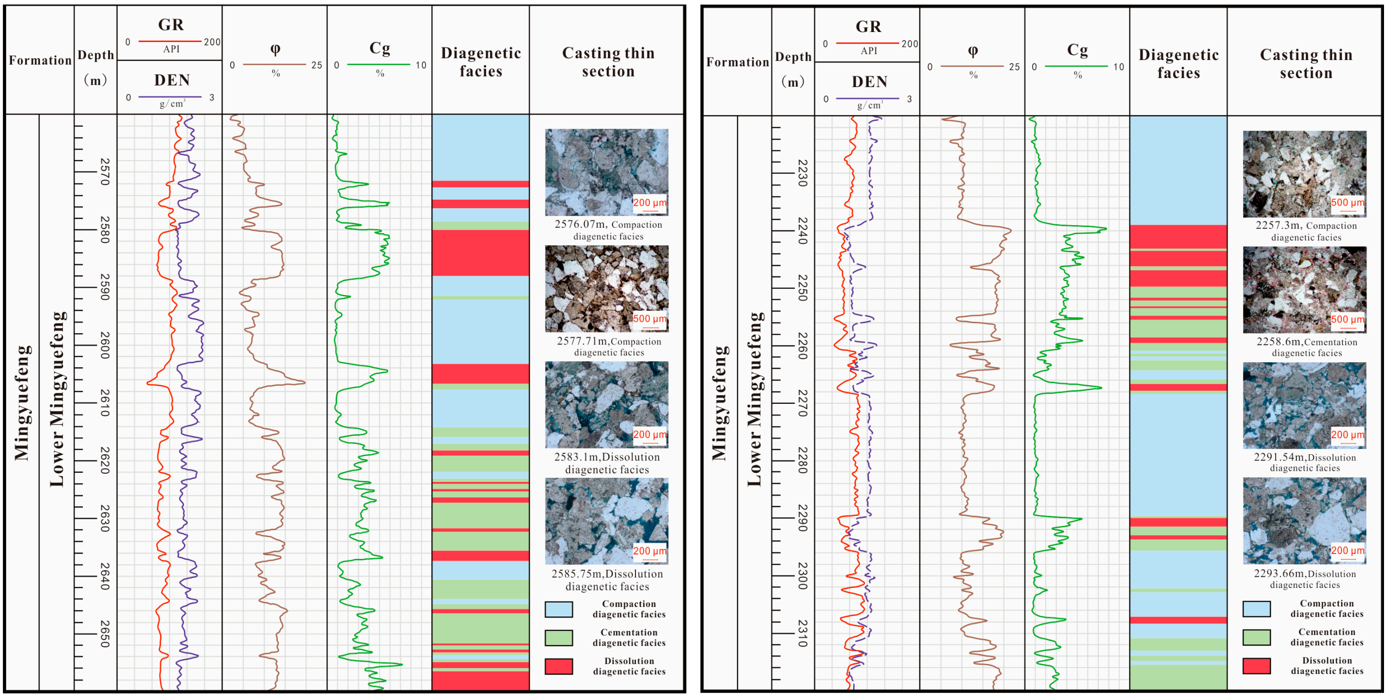

Figure 10. Vertical division of diagenetic facies of the Paleocene well L1 and L2.

The location of the L3 well is similar to that of the L1 and L2 wells, and the burial depth of the Paleocene reservoir is also between 2000 and 5000 m. The reservoir diagenetic facies are mainly compaction and cementation facies, which can reach a maximum thickness of 8.3 m. The dissolution facies is less developed, and the continuity is poor. Casting thin sections show that the pores after dissolution of plant fragments are filled with ferrocalcite. The compacted facies casting thin section can be seen with dense grains; ferrodolomite fills some pores (Figure 11).

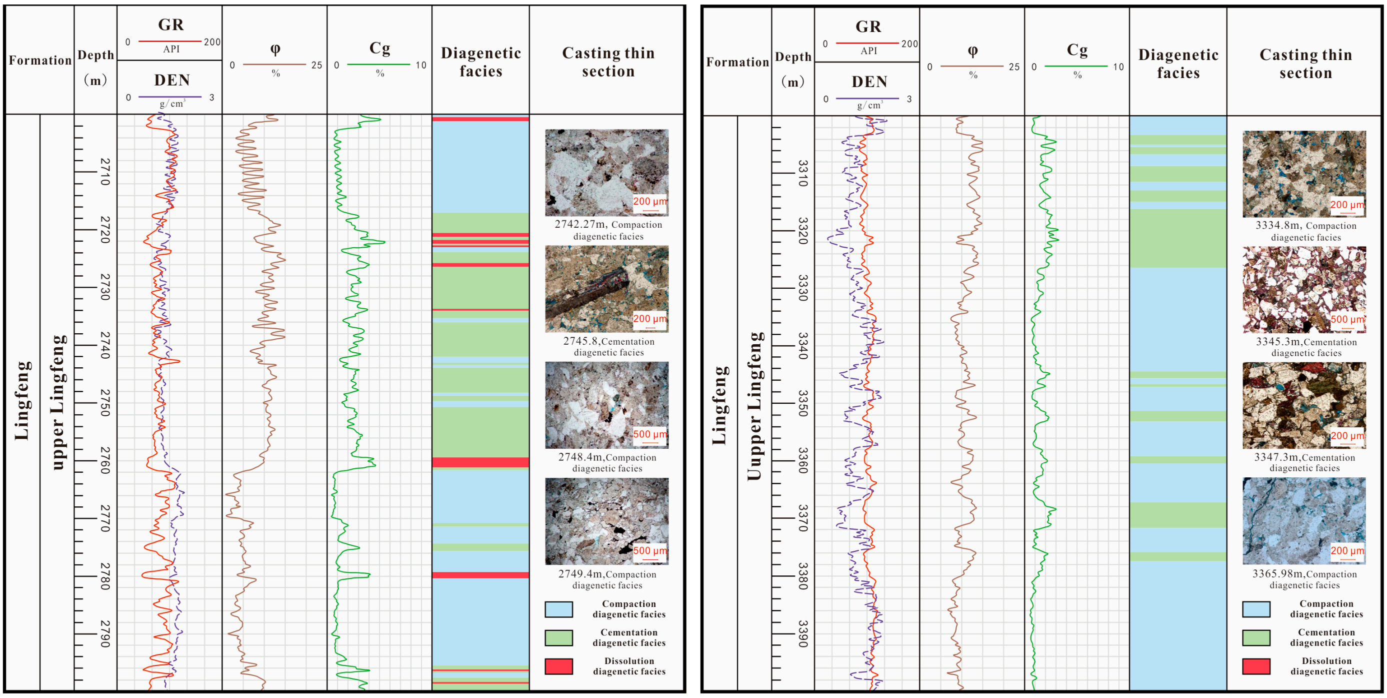

Figure 11. Vertical division of diagenetic facies of the Paleocene well L3 and L4.

The L4 well is located in the western ramp zone of the LS36 subsag in Lishui West Sag, with a buried depth of Paleocene reservoirs ranging from 1500 to 3700 m. The diagenetic facies of the reservoir are mainly compaction facies, with good continuity of cementation facies, and undeveloped dissolution facies. This may be due to the deep sampling location, where the dissolution pores have been filled with cement. The casting thin section shows typical characteristics of compaction facies and cementation facies. The grains in the compaction facies of the casting thin section are mainly in concave–convex contact, with fewer pores, which are micro-pores and cracks. The cementation facies of the casting thin section has a large area of development of cement, and it can be seen that ferrocalcite fills the pores extensively (Figure 11).

The L5 well is located on the Lingfeng Ridge on the east side of the Lishui West Sag. The Paleocene reservoir is buried between 2200 and 2500 m deep, and the diagenetic facies of the reservoir is mainly cementation facies. Directional compaction can be seen in the casting thin section of the compaction facies, with the grains mainly in concave–convex contact. The thin cast sections of the dissolution facies mainly develop intergranular dissolved pores, and the casting thin section of the compaction facies can be filled with ferrodolomite pores (Figure 12).

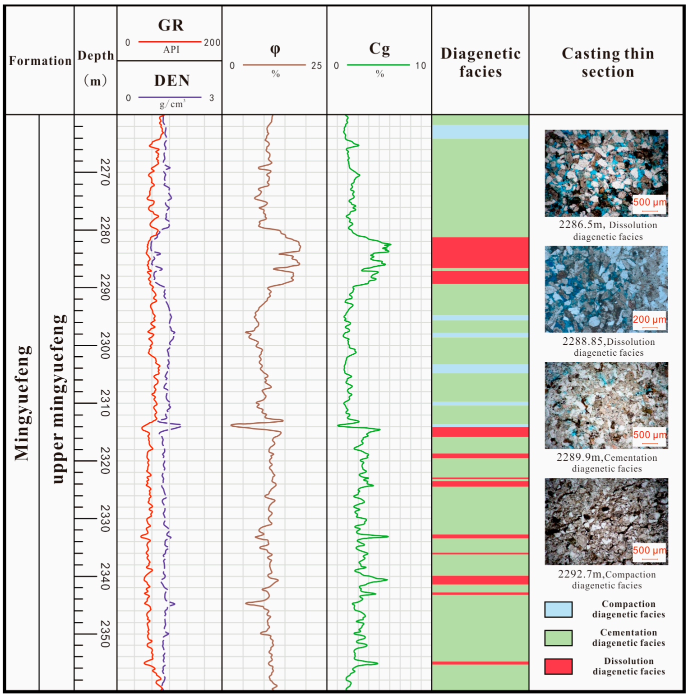

Figure 12. Vertical division of diagenetic facies of the Paleocene well L5.

5.4. Implications of Diagenetic Facies Control on Reservoir Quality for Hydrocarbon Exploration

Since the discovery of the Lishui L1 gas field in 1997, there has been little significant progress in the Lishui Sag. The main reason is the lack of shallow structural targets, and the deep burial of the Lingfeng Formation makes the reservoir difficult to predict. The prediction and identification of high-quality reservoirs in deep layers mainly depend on geophysical methods. However, dividing into lithofacies may be an effective method to distinguish the quality of reservoirs and improve the accuracy of reservoir prediction.

In the L1 gas field, the main reservoirs of wells L1, L2, and L3 are located in the lower section of the Mingyue Peak Group, at a depth of about 2500 m. This part of the stratum is characterized by a well-developed dissolution phase, thus forming a high-quality reservoir. In addition, there are fracture channels between the Mingyuefeng Group reservoir and the Yueguifeng Group source rocks, providing superior conditions for the migration of hydrocarbons. Furthermore, the thick mudstone layer covering the lower section of the

Mingyuefeng Group forms a good cap rock, thereby constructing an effective source–reservoir–cap combination. The dissolution phase in the dominant reservoir is mainly composed of large-grained, well-sorted sediments. Its burial depth is between 2200 and 2700 m and it is in the early stage of diagenesis. The main diagenetic minerals are calcite and kaolinite accompanied by feldspar dissolution. These minerals only fill a small amount of pores in the reservoir, and their impact on the porosity and permeability of the reservoir is negligible. In contrast, the reservoir of well L4 is developed at a deeper position, mainly manifested in the development of compaction and cementation phases. Additionally, well L4 is located on the western slope of the LS36 subsag, far from the source rocks. This location means that an extremely strong lateral conduction capacity is needed to form a gas reservoir. Consequently, no gas output is produced. For well L5, located in the east Lingfeng ridge zone of the Lishui West Sag, there are only stratum deposits in the upper part of the Mingyuefeng Group. Although it is close to the source rocks and there is fracture communication, the abundant development of the cementation phase and its strong cementation action prevent the formation of high-quality reservoirs.

6. Conclusions

(1) Using quantitative characterization parameters such as apparent compaction rate and apparent cementation rate, and incorporating the diagenetic comprehensive coefficient method, a standard for the quantitative division of the diagenetic facies of the Paleocene reservoirs in the Lishui West Sag was established. The diagenetic facies of these reservoirs were classified into three distinct types: compaction facies, cementation facies, and dissolution facies.

(2) The diagenetic comprehensive coefficient (C_g) of the Paleocene reservoirs in Lishui West Sag was matched with logging curve parameters, establishing a logging calculation model for the diagenetic comprehensive coefficient. This model enabled continuous quantitative identification and division of vertical diagenetic facies in individual well reservoirs using logging data. The effectiveness of the model was subsequently validated through thin-section analysis and physical property data.

(3) Continuous quantitative identification of vertical diagenetic facies in individual well reservoirs revealed that high-quality Paleocene reservoirs in Lishui West Sag are primarily concentrated in the LS36 subsag, where wells L1, L2, and L3 are located, characterized by an extensive development of dissolution facies. Considering the region's advantageous hydrocarbon source rocks, source–reservoir fracture communication, and a thick layer of mudstone cap rock, it facilitated the formation of the L1 gas field. This proves a certain matching relationship between diagenetic facies and oil and gas enrichment, providing a new approach for the exploration of high-quality deep reservoirs in the Paleocene of the Lishui West Sag.

Author Contributions: Conceptualization, J.T.; methodology, Q.F. and G.Z.; software, W.M.; validation, G.Z.; investigation, J.T.; resources, J.Q.; data curation, J.T.; writing—original draft preparation, J.T.; writing—review and editing, Q.F.; visualization, K.F.; supervision, J.Q.; project administration, W.M.; funding acquisition, Q.F. All authors have read and agreed to the published version of the manuscript.

Funding: This research received no external funding.

Data Availability Statement: Due to the nature of this research, participants of this study did not agree for their data to be shared publicly.

Acknowledgments: We thank the Shanghai Branch Company of CNOOC (China) for the provision of geological data and borehole samples. The careful review and constructive suggestions of the manuscript by anonymous reviewers are greatly appreciated.

Conflicts of Interest: Wenrui Ma is an employee of Shanghai Branch Company of CNOOC (China) Ltd,. The paper reflects the views of the scientists and not the company. The authors declare no any related conflicts of interest.

References

1. Lai, J.; Wang, G.; Wang, S.; Cao, J.; Li, M.; Pang, X.; Zhou, Z.; Fan, X.; Dai, Q.; Yang, L.; et al. Review of diagenetic facies in tight sandstones: Diagenesis, diagenetic minerals, and prediction via well logs. *Earth-Sci. Rev.* **2018**, *185*, 234–258. [CrossRef]
2. De Segonzac, G.D. The birth and development of the concept of diagenesis (1866–1966). *Earth-Sci. Rev.* **1968**, *4*, 153–201. [CrossRef]
3. Zhang, Y.L.; Bao, Z.D.; Zhao, Y.; Jiang, L.; Zhou, Y.Q.; Gong, F.H. Origins of authigenic minerals and their impacts on reservoir quality of tight sandstones: Upper Triassic Chang-7 Member, Yanchang Formation, Ordos Basin, China. *Aust. J. Earth Sci.* **2017**, *64*, 519–536. [CrossRef]
4. Zhang, Y.; Pe-Piper, G.; Piper, D.J. How sandstone porosity and permeability vary with diagenetic minerals in the Scotian Basin, offshore eastern Canada: Implications for reservoir quality. *Mar. Pet. Geol.* **2015**, *63*, 28–45. [CrossRef]
5. Wu, D.; Liu, S.; Chen, H.; Lin, L.; Yu, Y.; Xu, C.; Pan, B. Investigation and prediction of diagenetic facies using well logs in tight gas reservoirs: Evidences from the Xu-2 member in the Xinchang structural belt of the western Sichuan Basin, western China. *J. Pet. Sci. Eng.* **2020**, *192*, 107326. [CrossRef]
6. Zou, C.N.; Tao, S.Z.; Hui, Z.; Zhang, X.X.; He, D.B.; Zhou, C.M.; Lan, W.; Wang, X.S.; Li, F.H.; Zhu, R.K.; et al. Genesis, classification, and evaluation method of diagenetic facies. *Pet. Explor. Dev.* **2008**, *35*, 526–540. [CrossRef]
7. Zeng, H.; Zhu, X.; Zhu, R.; Zhang, Q. Seismic prediction of sandstone diagenetic facies: Applied to Cretaceous Qingshankou Formation in Qijia Depression, Songliao Basin, East China. *Pet. Explor. Dev.* **2013**, *40*, 287–295. [CrossRef]
8. Mansurbeg, H.; Morad, S.; Salem, A.; Marfil, R.; El-Ghali, M.; Nystuen, J.; Caja, M.; Amorosi, A.; Garcia, D.; La Iglesia, A. Diagenesis and reservoir quality evolution of palaeocene deep-water, marine sandstones, the Shetland-Faroes Basin, British continental shelf. *Mar. Pet. Geol.* **2008**, *25*, 514–543. [CrossRef]
9. Ajdukiewicz, J.M.; Lander, R.H. Sandstone reservoir quality prediction: The state of the art. *AAPG Bull.* **2010**, *94*, 1083–1091. [CrossRef]
10. Nguyen, B.T.T.; Jones, S.J.; Goulty, N.R.; Middleton, A.J.; Grant, N.; Ferguson, A.; Bowen, L. The role of fluid pressure and diagenetic cements for porosity preservation in Triassic fluvial reservoirs of the Central Graben, North Sea. *AAPG Bull.* **2013**, *97*, 1273–1302. [CrossRef]
11. Cui, Y.; Wang, G.; Jones, S.J.; Zhou, Z.; Ran, Y.; Lai, J.; Li, R.; Deng, L. Prediction of diagenetic facies using well logs—A case study from the upper Triassic Yanchang Formation, Ordos Basin, China. *Mar. Pet. Geol.* **2017**, *81*, 50–65. [CrossRef]
12. Ozkan, A.; Cumella, S.P.; Milliken, K.L.; Laubach, S.E. Prediction of lithofacies and reservoir quality using well logs, Late Cretaceous Williams Fork Formation, Mamm Creek field, Piceance Basin, Colorado. *AAPG Bull.* **2011**, *95*, 1699–1723. [CrossRef]
13. Zhang, X.; Zou, C.; Zhu, R.; Tao, S.; Yang, S. Reservoir diagenetic facies of the Upper Triassic Xujiahe Formation in the central Sichuan Basin. *Acta Pet. Sin.* **2011**, *32*, 257–264.
14. Yujiang, S.; Liang, X.; Zhiqiang, M.; Haopeng, G. An identification method for diagenetic facies with well logs and its geological significance in low-permeability sandstones: A case study on Chang 8 reservoirs in the Jiyuan region, Ordos Basin. *Acta Pet. Sin.* **2011**, *32*, 820–828.
15. Liu, H.; Zhao, Y.; Luo, Y.; Chen, Z.; He, S. Diagenetic facies controls on pore structure and rock electrical parameters in tight gas sandstone. *J. Geophys. Eng.* **2015**, *12*, 587–600. [CrossRef]
16. Lai, J.; Fan, X.; Liu, B.; Pang, X.; Zhu, S.; Xie, W.; Wang, G. Qualitative and quantitative prediction of diagenetic facies via well logs. *Mar. Pet. Geol.* **2020**, *120*, 104486. [CrossRef]
17. Li, Y.; Zhang, J.; Liu, Y.; Shen, W.; Chang, X.; Sun, Z.; Xu, G. Organic geochemistry, distribution and hydrocarbon potential of source rocks in the Paleocene, Lishui Sag, East China Sea Shelf Basin. *Mar. Pet. Geol.* **2019**, *107*, 382–396. [CrossRef]
18. Liu, J. Fine description of structure research of Lishui sag, East China Sea Basin. *Arab. J. Geosci.* **2014**, *8*, 4433–4441. [CrossRef]
19. Lei, C.; Yin, S.; Ye, J.; Wu, J.; Wang, Z.; Gao, B. Characteristics and deposition models of the paleocene source rocks in the Lishui Sag, east China sea shelf basin: Evidences from organic and inorganic geochemistry. *J. Pet. Sci. Eng.* **2021**, *200*, 108342. [CrossRef]
20. Zhang, M.; Zhang, J.; Xu, F.; Li, J.; Liu, J.; Hou, G.; Zhang, P. Paleocene sequence stratigraphy and depositional systems in the Lishui Sag, East China Sea Shelf Basin. *Mar. Pet. Geol.* **2015**, *59*, 390–405. [CrossRef]
21. Lai, J.; Wang, G.; Cai, C.; Fan, Z.; Wang, S.; Chen, J.; Luo, G. Diagenesis and reservoir quality in tight gas sandstones: The fourth member of the Upper Triassic Xujiahe Formation, Central Sichuan Basin, Southwest China. *Geol. J.* **2017**, *53*, 629–646. [CrossRef]
22. Fa, X.; Penghui, Z.; Jinliang, Z.; Jinshui, L.; Guowei, H.; Ming, Z.; Jingzhe, L.; Shasha, L.; Jiaqi, G.; Ningning, M. Diagenesis and Diagenetic Evolution of Deltaic and Neritic Gas-Bearing Sandstones in the Lower Mingyuefeng Formation of Paleogene, Lishui Sag, East China Sea Shelf Basin: Implications for Depositional Environm. *Acta Geol. Sin.* **2015**, *89*, 1625–1635. [CrossRef]
23. Liu, L.; Li, Y.; Dong, H.; Sun, Z. Diagenesis and reservoir quality of Paleocene tight sandstones, Lishui Sag, East China Sea Shelf Basin. *J. Pet. Sci. Eng.* **2020**, *195*, 107615. [CrossRef]
24. Liang, J.; Wang, H. Cenozoic tectonic evolution of the East China Sea Shelf Basin and its coupling relationships with the Pacific Plate subduction. *J. Asian Earth Sci.* **2019**, *171*, 376–387. [CrossRef]
25. Xu, F.; Zhang, P.H.; Zhang, J.L.; Zhang, M. Diagenetic Facies in Paleocene Sandstones, Lishui Sag, East China Sea. *Adv. Mater. Res.* **2013**, *807–809*, 2170–2173. [CrossRef]
26. Sun, Z.; Zhang, J.; Liu, Y.; Shen, W.; Li, Y.; Li, L. Sedimentological Signatures and Identification of Sedimentary Facies of the Paleocene in the Lishui Sag, East China Sea Shelf Basin. *Can. J. Earth Sci.* **2019**, *57*, 377–395. [CrossRef]

27. Huang, Y.; Tarantola, A.; Wang, W.; Caumon, M.-C.; Pironon, J.; Lu, W.; Yan, D.; Zhuang, X. Charge history of CO_2 in Lishui sag, East China Sea basin: Evidence from quantitative Raman analysis of CO_2-bearing fluid inclusions. *Mar. Pet. Geol.* **2018**, *98*, 50–65. [CrossRef]
28. Fu, C.; Li, S.; Li, S.; Xu, J.; Huang, Y. Genetic types of mudstone in a closed-lacustrine to open-marine transition and their organic matter accumulation patterns: A case study of the paleocene source rocks in the east China sea basin. *J. Pet. Sci. Eng.* **2022**, *208*, 109343. [CrossRef]
29. Liu, J.S.; Zhang, M.; Zhang, J.L.; Wang, C.Y.; Zhang, P.H. Tectonic Evolution and Sequence Filling of Paleocene in Lishui Sag, East China Sea Shelf Basin. *Adv. Mater. Res.* **2013**, *807–809*, 2244–2248. [CrossRef]
30. Han, X.; Hou, D.; Cheng, X.; Li, Y. Impact of Terrigenous Organic Matter Input on Organic Matter Enrichment of Paleocene Source Rocks, Lishui Sag, East China Sea. *Energies* **2023**, *16*, 2046. [CrossRef]
31. Su, A.; Chen, H.; Cao, L.; Lei, M.; Wang, C.; Liu, Y.; Li, P. Genesis, source and charging of oil and gas in Lishui sag, East China Sea Basin. *Pet. Explor. Dev.* **2014**, *41*, 574–584. [CrossRef]
32. Hou, G.; Liu, J.; Cai, K.; Wang, Y. Analysis of Sandbody Development Model in Lishui Depression. *Earth Sci. Res.* **2018**, *7*, 18–24. [CrossRef]
33. Houseknecht, D.W. Assessing the relative importance of compaction processes and cementation to reduction of porosity in sandstones. *AAPG Bull.* **1987**, *71*, 501–510.
34. Hongkun, L.; Yong, A.; Guiwen, W.; Kangjun, C.; Deyang, C.; Juntao, C.; Yuqiang, X.; Dong, L.; Jin, L. Quantitative well logging evaluation of diagenetic facies of deep and ultra deep tight sandstone reservoirs: A case study of Bozi-Dabei area in Kuqa Depression. *Bull. Geol. Sci. Technol.* **2023**, *42*, 299–310.
35. Ning, Y.A.; Guiwen, W.A.; Chaoliu, L.I. Reservoir diagenetic facies of Bashijiqike Formation in Dabei gas field compartmentalization and quantitative evaluation. *J. China Univ. Pet.* **2014**, *38*, 18–24.
36. Ziqi, S.; Jing, W.; Xiangwei, L.; Xiaolong, Y.; Lilei, Y.; Hongyu, Z. Speciallow permeability reservoir diagenetic reservoir faciesquantitative evaluation method. *Pet. Geol. Recovery Efficiecy* **2006**, *13*, 21–23.
37. Qigui, C.; Lei, Z.; Haini, Z.; Fuhua, G. Based on the diagenesis of quantitative characterizationof diagenetic reservoir facies classification and signifi-cance. *J. Pet. Nat. Gas* **2010**, *32*, 60–65.
38. Lai, J.; Wang, G.; Chai, Y.; Ran, Y.; Zhang, X. Depositional and Diagenetic Controls on Pore Structure of Tight Gas Sandstone Reservoirs: Evidence from Lower Cretaceous Bashijiqike Formation in Kelasu Thrust Belts, Kuqa Depression in Tarim Basin of West China. *Resour. Geol.* **2015**, *65*, 55–75. [CrossRef]
39. Li, Y.; Qiao, W.; Yang, X.; Wu, Y.; Li, X.; Zhang, S. A Comprehensive Classification Method for the Pore Permeability of Deep-Mine Sandstone Used to Guide Grouting. *Appl. Sci.* **2023**, *13*, 1840. [CrossRef]
40. Zhu, P.; Dong, Y.; Chen, M.; Li, Z.; Han, B.; Wang, J.; Cui, Y. Quantitative evaluation of pore structure from mineralogical and diagenetic information extracted from well logs in tight sandstone reservoirs. *J. Nat. Gas Sci. Eng.* **2020**, *80*, 103376. [CrossRef]
41. Carvalho, M.V.F.; Ros, L.F.D.; Gomes, N.S. Carbonate cementation patterns and diagenetic reservoir facies in the Campos Basin Cretaceous turbidites, offshore eastern Brazil. *Mar. Pet. Geol.* **1995**, *12*, 741–758. [CrossRef]
42. Rushing, J.A.; Newsham, K.E.; Blasingame, T.A. Rock Typing: Keys to Understanding Productivity in Tight Gas Sands. *J. Pet. Technol.* **2008**, *60*, 53–54.
43. Guo-min, F.; Xiao-li, Q.; Qing, M.; Tian-jin, Z.; Jian-peng, Y. Division of diagenesis reservoir facies and its control—Case study of Chang-3 reservoir in Yangchang formation of Fuxian exploration area in northern Shaanxi. *Min. Sci. Technol.* **2009**, *19*, 0537–0543.
44. Shirley, D.P.F.; Robert, L.G. Diagenetic controls on evolution of porosity and permeability in lower Tertiary Wilcox sandstones from shallow to ultradeep (200–6700 m) burial, Gulf of Mexico Basin, U.S.A. *Mar. Pet. Geol.* **2010**, *27*, 69–81.
45. Lai, J.; Wang, G.; Chai, Y.; Xin, Y.; Wu, Q.; Zhang, X.; Sun, Y. Deep burial diagenesis and reservoir quality evolution of high-temperature, high-pressure sandstones: Examples from Lower Cretaceous Bashijiqike Formation in Keshen area, Kuqa depression, Tarim basin of China. *AAPG Bull.* **2017**, *101*, 829–862. [CrossRef]